

PACS numbers: 42.30.Wb; 87.64.Cc; 87.63.L–; 42.62.Be
DOI: 10.1070/QE2012v042n06ABEH014883

Raster scanning and averaging for reducing the influence of speckles in optical coherence tomography

S.G. Proskurin

Abstract. **The application of small-angle raster scanning and averaging in the sample arm of the Michelson interferometer in optical coherence tomography (OCT) is described. Raster averaging is used to increase the signal-to-noise ratio and to reduce the speckle noise of the 2D OCT image in diagnostics of surface layers of human skin and subcutaneous blood vessels *in vivo*. The method allows using low-coherence source of low-power radiation and increasing the depth of human skin coherent probing up to 1.5–1.8 mm. The reduction of speckle noise in the obtained OCT image for the first time allowed visualisation of subcutaneous blood vessels at the entire depth of their localisation.**

Keywords: *optical coherence tomography, coherence probing depth, optical properties of skin, blood vessels.*

1. Introduction

Optical spectroscopy and tomography are based on measuring absorption, scattering and reflection of near-IR radiation having the wavelength $\lambda = 700–1500$ nm. The wavelengths in the range 800–1300 nm are used most often. The optical diagnostic using low (smaller than one milliwatt) radiation intensities is considered to be a harmless noninvasive technique of biomedical investigation, in contrast to X-ray imaging methods [1].

Optical coherence tomography (OCT) appeared in late eighties – early nineties of the twentieth century [2]. In the beginning of the twenty-first century it holds an important position among the biomedical diagnostic methods [3]. OCT makes use of the optical signal, reflected from surfaces with different optical densities, and it is to a large extent analogous to the ultrasonic (US) diagnostics.

For surface layers of human skin, in which the reduced coefficient of optical radiation scattering is $\mu_s' \sim 1$ mm^{-1}, the probing depth of standard OCT systems is 1.0–1.2 mm, which is essentially smaller than in US investigations [4, 5] and in X-ray instruments [6]. Because of strong scattering of optical radiation in biotissue, OCT systems are commonly used in the studies of cornea, vitreous humour and retina of the eye (in medicine the appropriate instruments are referred as retinal tomographs). However, the resolution of OCT systems in similar studies is by one–two orders of magnitude higher than that of US systems. For the latter the resolution amounts to 100 μm–1 mm [5].

In optical low-coherence reflectometry the principles of scanning low-coherence interferometry are used [7, 8]. The low coherence of the radiation source is due to its broad spectral band ($\Delta\lambda$), which yields high longitudinal spatial resolution in the schemes of scanning interferometers

$$\Delta z = \frac{2\ln 2}{\pi}\frac{\lambda^2}{\Delta\lambda} \approx 0.44\frac{\lambda^2}{\Delta\lambda}.$$

With cw superluminescent diodes (SLD) having $\lambda = 800–1700$ nm and the spectral bandwidth $\Delta\lambda = 20–100$ nm the localisation of the longitudinal component of the measurement volume (i.e., the spatial resolution with respect to the probing depth Δz) approaches 5–15 μm. Since the radiation propagates through biological tissues, the refractive index $n \approx 1.4$ [9] of the latter should be taken into account. This improves the spatial resolution in a biological object: $L_{ax}=\Delta z/n \sim 4–11$ μm.

As a rule, the techniques of OCT studies is based on using the scheme of a scanning Michelson interferometer, implemented on the basis of single-mode optical fibres (Fig. 1), or Linnik microscope [10].

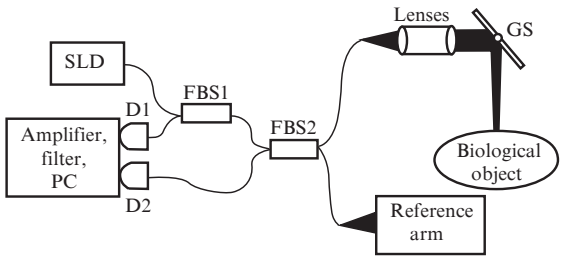

Figure 1. Scheme of optical coherence tomograph implemented on the base of single-mode optical fibres: (FBS1, FBS2) fibre beam splitters 1 × 2 and 2 × 2; (GS) galvanic scanner; (D1, D2) IR radiation detectors, incorporated in a balance scheme; a modified rapid scanning optical delay (RSOD) line is included into the reference arm.

Compared to the quasi-elastic scattering, where a narrowband radiation source is used (a laser with $\Delta\lambda \sim 0.1–1$ nm), in the scheme with a low-coherence source besides the coherent interference signal an incoherent parasitic signal that manifests itself as a phase noise [7, 10] is also recorded.

The strength of the electric fields $\tilde{E}_r = E_r\cos(kz_r + \varphi_1)$ and $\tilde{E}_s = E_s\cos(kz_s + \varphi_2)$ coming from the reference and sample arms of the Michelson interferometer, respectively, produce

S.G. Proskurin Tambov State Technical University, ul. Sovetskaya 106, 392000 Tambov, Russia; e-mail: spros@tamb.ru

Received 14 May 2012
Kvantovaya Elektronika **42** (6) 495–499 (2012)
Translated by V.L. Derbov

the intensity of the recorded radiation on the balance quadratic photodetector that can be written as

$$I = \langle (E_r + E_s)^2 \rangle = I_{in} + E_r^2 + E_s^2 + 2E_rE_s \times \cos[2\pi f_0 t + (\varphi_1 - \varphi_2)],$$

where I_{in} is the incoherent component of the signal (phase noise). Using one detector in the heterodyne regime one should increase the intensity of the reference radiation $I_r = E_r^2$ in order to increase the signal-to-noise ratio. In this case, the sum of intensities in the reference and sample arms of the interferometer $I_r + I_s = E_r^2 + E_s^2$ will increase, too. In the regime of signal detection by means of two photodetectors, incorporated in a balance scheme, in order to reduce the phase noise one should decrease the radiation intensity in the reference arm [11].

The carrier frequency of the scanning interferometer f_0, at which the filtering and detection of the signal is performed, corresponds to the classical Doppler shift, arising due to the mirror in the reference arm moving with the velocity V:

$$f_0 = 2V/\lambda.$$

With the linear scanning optical delay line (ODL) the amplification bandwidth of the signal filter Δf is approximately equal to the line broadening, proportional to the bandwidth of the broadband source ($\Delta\lambda \sim 20-300$ nm):

$$\Delta f = f_0 \Delta\lambda/\lambda.$$

In the case of using the Fourier rapid scanning optical delay (RSOD) line [11, 12] the transmission bandwidth is given by the following expression:

$$\Delta f = K \frac{\Delta\lambda}{\lambda^2} \frac{\partial\alpha}{\partial t},$$

where $\partial\alpha/\partial t$ is the angular velocity of the scanning mirror in the reference arm; α is the instantaneous value of the mirror scanning angle. The coefficient K depends on the RSOD parameters and approximately equals 4, which corresponds to the increase in the transmission bandwidth in the case of RSOD by nearly four times as compared with the case of linearly scanning mirror [12].

The rapidly scanning optical delay line was initially developed for measuring the shape and duration of ultrashort laser pulses, which implies the use of high-power radiation sources. In [11, 13] RSOD was first modified so that the power of radiation, introduced into each arm of the interferometer, was reduced to 0.1–0.2 mW. Further reduction of SLD power has no sense because in this case the electric noises of the amplifier become comparable with speckle noises and noises of the radiation source.

Increasing the group velocity in the linear optical delay line causes unavoidable increase in the phase velocity, which leads to an increase in the carrier frequency f_0. RSOD allows separation of the group and phase velocity tuning, i.e., independent tuning of the carrier frequency within the limits from zero to a few hundred kilohertz, keeping the scanning rapid enough. The construction of RSOD [11] used here allows detuning from high-frequency white noise and shifting the carrier frequency into the region of a few tens of kilohertz. The analysis of noises present in the signal spectrum allowed determination of the optimal carrier frequency equal to 25 kHz.

Similar to US diagnostic methods, OCT images are subject to speckle noise due to the partial coherence of the radiation used. It is observed in the form of spots (speckles) in the two-dimensional image, reconstructed by means of computer software, which in analogy with US imaging is referred as B-scan. Each B-scan contains numerous (from a few tens to a few hundred) A-scans, i.e., individual interferograms of the scanning interferometer.

The aim of the present paper is to increase the coherence probing depth in OCT by using small-angle raster scanning in the sample arm followed by averaging over groups of adjacent A-scans.

2. Materials and methods

In the experiment (Fig. 1) the radiation from the SLD (λ = 1298 nm, $\Delta\lambda$ = 52nm) arrives at the fibre beam splitter FBS1 and then at the second fibre beam splitter FBS2. From the latter half of the radiation is directed into the reference arm of the interferometer, while the second half enters the sample arm and is focused onto the sample by means of a system of lenses. The radiation reflected from both arms of the interferometer is mixed on balance quadratic photodetectors D1 and D2. After the balance scheme the electric signal passes the controllable bandpass filter and then the spectrum analyser and analogue-to-digital converter (ADC). After the ADC the digital signal is recorded and processed by the computer. To obtain a 2D image the scanning in the sample arm by means of the second galvanic scanner is used.

Traditionally in OCT systems the parallel scanning of the sample stage was used, when the stage with the studied object was moved stepwise in the direction, perpendicular to that of the radiation propagation in the sample arm (Fig. 2).

In the studies of biomedical objects *in vivo* in the sample arm they often use the angle scanning of the mirror, placed in

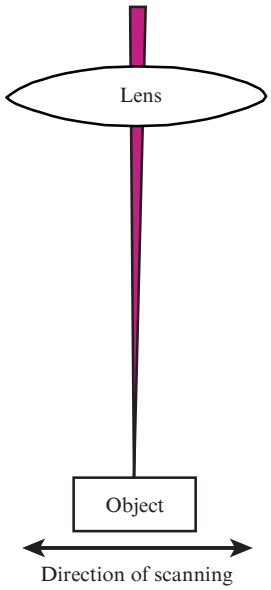

Figure 2. Scheme of parallel scanning of the object stage in the sample arm of optical coherence tomograph.

front of the focusing lens, or scanning of the lens itself (Fig. 3), which yields an increase in the signal-to-noise ratio by 1.5–2 times [14, 15]. Such a geometry is used to focus the radiation and to obtain the minimal transverse spatial resolution of 5–20 μm [15]. Low-coherence radiation may be focused into a spot of smaller size, than the radiation with high coherence. Experiments have shown that such focusing does not allow the coherence probing depth higher than 1.0–1.2 mm in surface layers of human skin [11, 14].

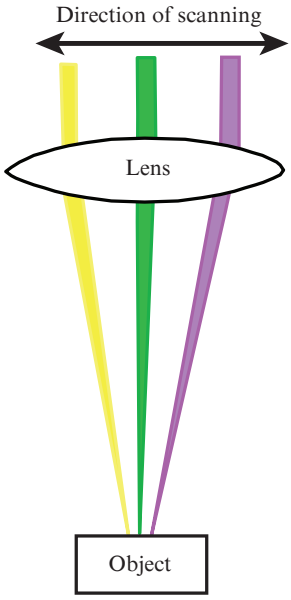

Figure 3. Scheme of angle scanning of the probing radiation in te sample arm of optical coherence tomograph [14].

In the present paper we use the scheme of remote raster scanning (Fig. 4). The distance from the scanning mirror and lens system with a small numerical aperture NA to the object amounts to 8–12 cm, which is 4–10 times greater than the appropriate distance in standard schemes (Figs 2 and 3).

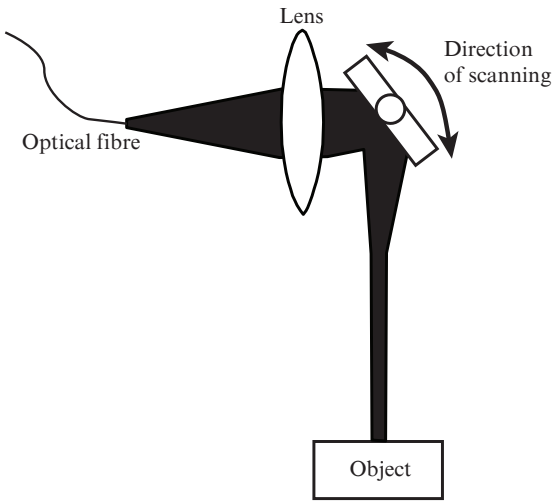

Figure 4. Scheme of small-angle raster scanning of probing radiation in the sample arm of the optical coherence tomograph [10].

In our scheme the transverse resolution is determined by the diameter of the waist of the focused beam $\omega = 1.22\lambda/(2\mathrm{NA})$ and increases up to 50–100 μm. This leads to a decrease in the spatial resolution by 3–5 times, but for imaging layered structures (nails, nail bed, subcutaneous structures) this resolution is quite enough. Moreover, choosing the numerical aperture of the focusing optics to be small makes it possible to avoid detection of photons, multiply scattered at large angles, and to select the reflected component alone, which contains information about the structure of the biological object. The axial resolution L_{ax} remains to be determined by the source coherence length and keeps unchanged (5–10 μm).

The choice of the SLD wavelength was determined by the fact that the maximal depth of penetration of radiation into a biological tissue is achieved at $\lambda \sim 1.3$ μm [9]. Moreover, a pulse shorter than 10 fs corresponds to a coherent wave packet as long as 3 μm. In a biological tissue such a short pulse causes an increase in dispersion of the optical radiation, which decreases the coherence probing depth. When the numerical aperture is decreased, the confocal parameter is simultaneously increased up to the value, corresponding to the coherence probing depth of 2–3 mm. In this case the maximal signal-to noise ratio is achieved.

In the described experiment the lengths of both reference and sample arms of the scanning interferometer vary continuously by means of galvanic scanners rather than stepwise as in the scheme presented in Fig. 2. It was empirically found that processing the interferograms by means of the fast Fourier transform with the shift of the Hanning window by 20%–30% yields the same contrast of the image, as processing of the signal with continuous shift. A more detailed description of the experimental setup, the algorithm of signal processing and image construction is presented in [11, 13].

3. Results and discussion

As a trial object we used the surface of the onion bulb (Allium cepa). The main object of study was the skin of a human finger *in vivo* with subcutaneous blood vessels visible to the naked eye.

Figure 5 shows substantial difference in contrast of the OCT images of the onion bulb (Allium cepa) surface produced by averaging over five adjacent A-scans in each vertical line of the image.

For biomedical objects we managed to obtain images of human subcutaneous blood vessels having the diameter 0.2–1 mm [11, 13]. Figure 6 shows a subcutaneous blood vessel with the diameter ~1 mm, located at the depth of 1–1.8 mm,

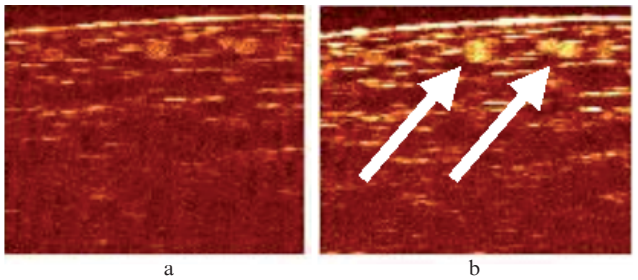

Figure 5. OCT images of the surface of the onion bulb (Allium cepa) before (a) and after (b) averaging. The arrows point at the structures that are clearly seen after the averaging. The image size is 1.8 × 1.8 mm.

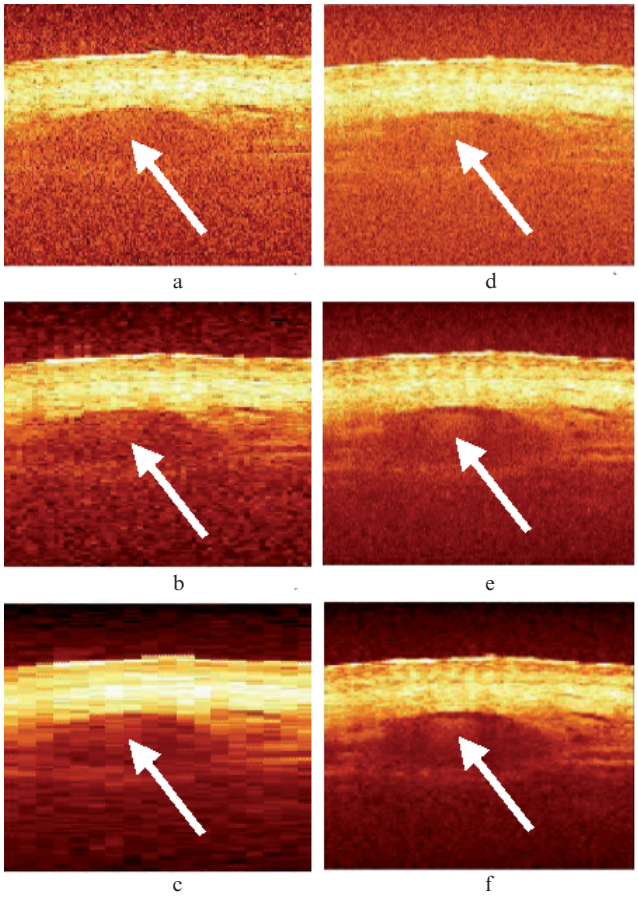

Figure 6. OCT images of skin and blood vessel of human finger *in vivo* before averaging (a, d) and after averaging over three (b, e) and ten (c, f) adjacent A-scans. The left images (a–c) have 180 original vertical A-scans and the right images (d–f) have 900 A-scans, i.e., five times greater number of scans. Arrows point at the location, where the structural image of blood is seen with contrast only after averaging. The image size is 2×2 mm.

before averaging, after averaging over each three and each ten adjacent A-scans. The images in Figs 6a–c are obtained using the file, containing 180 original vertical A-scans. Because of the small number of scans, after averaging over each ten adjacent scans we get a B-scan with a very low resolution, with 18 vertical lines only (Fig. 6c). As a result, the structure of the vessel becomes blurred; the image is destroyed and cannot be used for biomedical diagnostics.

The images in Figs 6d–f are produced from the file that contains five times as much, i.e., 900 original A-scans. The arrows point at the structural images of the vessel that appear in Figs 6e and f; a substantial improvement of contrast and reduction of speckle noise is seen. A further increase in the number of A-scans, over which the averaging is performed, worsens the image making pixels too large, like in Fig. 6c with the file having 180 vertical lines.

The signal-to-noise ratio was calculated in a standard way [15], namely, the ratio of the mean value of maximal intensity $\langle I \rangle$ of the reflected radiation to the standard deviation σ of the signal from a uniform region of the object was taken:

$$\mathrm{S/N} = \langle I \rangle / \sigma.$$

The region of uniformity was assessed by the ergodicity of the random process; namely, the lower, homogeneous part of the image was chosen, where the average values over time (of individual A-scans) and over realisations (of different A-scans at similar moments of time) coincided. Note, that this formula was chosen also because it is inverse to the other important quantitative characteristic, the speckle contrast

$$C = \sigma / \langle I \rangle.$$

The dependence of the signal-to-noise ratio on the number of adjacent A-scans involved in the averaging procedure is shown in Fig. 7a. The use of the logarithmic scale (Fig. 7b) makes it obvious that up to 60 A-scans in the averaged sample this dependence does not exhibit asymptotic saturation, and the experimental points rigorously lie on the straight line. The scanning of the lens in the sample arm studied in [15] (Fig. 3) shows that after averaging over 5–7 scans the dependence is asymptotically saturated and approaches a horizontal straight line (see Fig. 4 in [15]). In the experiment described in the present paper no such asymptotic saturation was observed.

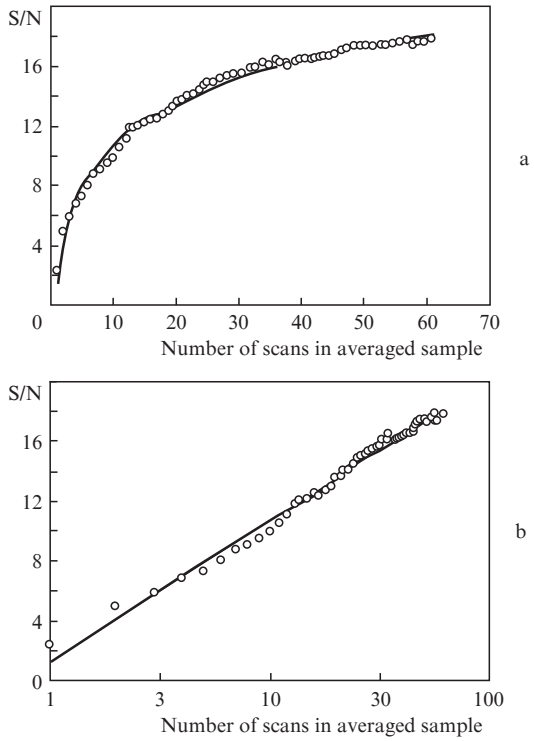

Figure 7. Dependences of signal-to-noise ratio S/N on the number of scans in the groups, over which the averaging is carried out, for small-angle raster scanning (see Fig. 4). The points are experimental data; the solid lines show the logarithmic approximation.

At the same time, for the file containing 180 lines the averaging over each 10–15 adjacent A-scans leads to strong blurring of the image. This means that taking the angle between the successive A-scans to be 10–15 times smaller and increasing the rate of data acquisition up to a few thousand lines per second, e.g., using the spectral OCT, it is possible to increase the coherence probing depth up to 2–2.5 mm. Such a result follows from the fact that the coherent back-reflected signal is 'lost' in the diffusely scattered signal only when the transport length $l^* = (\mu_s')^{-1}$ becomes equal to 2–2.5 mm in a scattering medium with optical properties, similar to those of human

skin [16]. Such coherence probing depth may be considered as the limit one, below which the intensity of the back-reflected coherent signal becomes equal to that of the backscattered diffuse signal.

Note that linear scanning of the object stage (see Fig. 2) followed by averaging yields an irregular behaviour of the signal-to-noise ratio in the experiments performed (Fig. 8). The explanation of this irregular character of the dependence will be a subject of future studies.

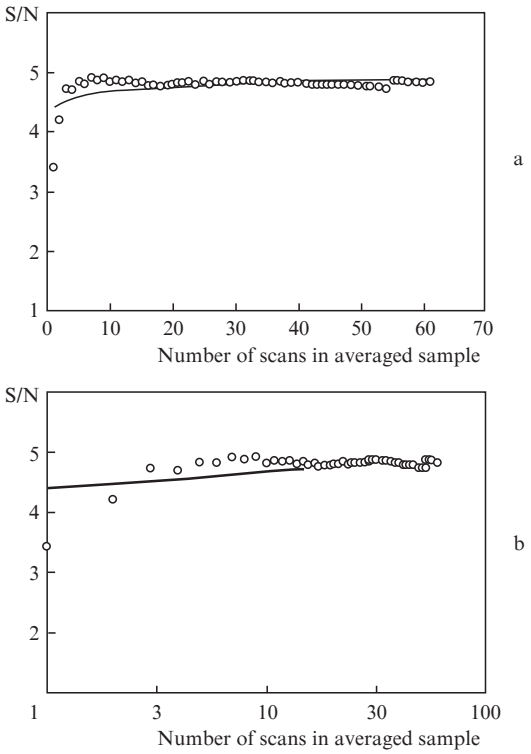

Figure 8. Dependences of signal-to-noise ratio S/N on the number of scans in the groups, over which the averaging is carried out, for linear scanning (see Fig. 2). The points are experimental data; the solid lines show the logarithmic approximation. Asymptotic saturation occurs after reaching the number of 5–7 scans in the averaged samples.

The processing of individual vertical lines has shown [11] that the axial resolution L_{ax} gradually worsens and varies from the theoretical value of 10 μm to 30–50 μm. This is due to the recording of backscattered radiation, which remains coherent to the radiation in the reference arm of the interferometer. Deeper layers of skin can be imaged by recording only photons scattered several times. This is an intermediate regime between the reflection and diffuse scattering signals [11, 16]. Here we mean the regime of detecting the photons, scattered a few times and still keeping coherence with the radiation in the reference arm of the interferometer.

4. Conclusions

In the present work in the reference arm of the OCT system we used the improved scanning optical delay line based on a diffraction grating that allowed shifting the carrier frequency f_0 into the low-frequency region with minimal noises (f_0 = 25 kHz). In the sample arm we used the remote small-angle raster scanning. The use of such scanning with subsequent averaging shows that with the number up to 60 of averaged scans, corresponding to different angles, no asymptotic saturation of the dependence of the signal-to-noise ratio on the number of averaged scans is observed.

Averaging over 5–10 A-scans allows elimination of speckles and provides maximal contrast of the image. In this case it appears possible to detect the photons in the intermediate regime between the back reflection and multiple diffusion scattering [16].

In the future we plan to compare the obtained experimental data with the results of Monte Carlo simulation of OCT images [17] and to explain the irregular character of the dependence of the signal-to-noise ratio on the number of averaged scans in the described experiment with linear scanning of the object stage. For the raster scanning it is necessary to find the optimal angle between the adjacent A-scans.

References

1. Schmidt F.E.W. *PhD Thesis* (University College, London, 1999).
2. Zimnyakov D.A., Tuchin V.V. *Kvantovaya Elektron*., **32** (10), 849 (2002) [*Quantum Electron*., **32** (10), 849 (2002)].
3. Gladkova N.D. *Opticheskaya kogerentnaya tomografiya v ryadu metodov meditsinskoy vizualizatsii: kurs lektsii* (Optical Coherence Tomography Among The Methods of Medical Imaging: A Lecture Course) (Nizhny Novgorod: Institute of Applied Physics RAS, 2005).
4. Gundorova R.A., Kvasha O.I., Nurmamedov R.A. *Rossiiskii obschenatsional'nyi forum. Sbornik trudov* (Russian National Forum. Collected Papers) (Moscow, 2008) p. 202.
5. Fisher Y.L., Nogueira F., Salles D., in *Diagnostic Ophthalmic Ultrasonography* (Philadelphia, Pa: Lippincott Williams & Wilkins, 2009).
6. Abahussin M., Hayes S., Knox N.E., Kamma-Lorger C.S., Khan Y., Marshall J., Meek K.M. *Invest. Ophthalmol. Vis. Sci*., **50** (11), 5159 (2009).
7. Fercher A.F., Roth E. *Proc. SPIE Int. Soc. Opt. Eng*., **658**, 48 (1986).
8. Youngquist R.C., Carr S., Davies D.E.N. *Opt. Lett*., **12** (3), 158 (1987).
9. Tuchin V.V. *Tissue Optics: Light Scattering Methods and Instruments for Medical Diagnostics* (Bellingham: SPIE Press, 2007).
10. Linnik V.P. *Izv. Akad. Nauk SSSR*, **1** (2), 210 (1933).
11. Proskurin S.G. *Adv. Life Sci.*, **1** (2), 40 (2011).
12. Rollins A., Izatt J., Kulkarni M., Yazdanfar S., Ung-Arunyawee R. *Opt. Express*, **3** (6), 219 (1998).
13. Proskurin S.G., Meglinski I.V. *Laser Phys. Lett*., **4** (11), 824 (2007).
14. Kennedy B.F., Hillman T.R., Curatolo A., Sampson D.D. *Opt. Lett*., **35** (14), 2445 (2010).
15. Desjardins A.E., Vakoc B.J., Oh W.Y., Motaghiannezam S.M.R., Tearney G.J., Bouma B.E. *Opt. Express*, **15** (10), 6200 (2007).
16. Hee M.R., Izatt J.A., Swanson E.A., Fujimoto J.G. *Opt. Lett*., **18** (13), 1107 (1993).
17. Kirillin M., Meglinski I., Kuzmin V., Sergeeva E., Myllylä R. *Opt. Express*, **18** (21), 21714 (2010).